NANO LETTERS

pubs.acs.org/NanoLett

Letter

Deep Learning-Powered Colloidal Digital SERS for Precise Monitoring of Cell Culture Media

Peng Zheng, Lintong Wu, Michael Ka Ho Lee, Andy Nelson, Michael Betenbaugh, and Ishan Barman*

Cite This: *Nano Lett.* 2025, 25, 6284−6291

Read Online

ACCESS | Metrics & More | Article Recommendations | Supporting Information

ABSTRACT: Maintaining consistent quality in biomanufacturing is essential for producing high-quality complex biologics. Yet, current process analytical technologies (PAT) often fall short in achieving rapid and accurate monitoring of small-molecule critical process parameters and critical quality attributes. Surface-enhanced Raman spectroscopy (SERS) holds great promise but faces challenges like intensity fluctuations, compromising reproducibility. Herein, we propose a deep learning-powered colloidal digital SERS platform. This innovation converts SERS spectra into binary "ON/OFF" signals based on defined intensity thresholds, which allows single-molecule event visualization and reduces false positives. Through integration with deep learning, this platform enables detection of a broad range of analytes, unlimited by the lack of characteristic SERS peaks. Furthermore, we demonstrate its accuracy and reproducibility for studying AMBIC 1.1 mammalian cell culture media. These results highlight its rapidity, accuracy, and precision, paving the way for widespread adoption and scale-up as a novel PAT tool in biomanufacturing and diagnostics.

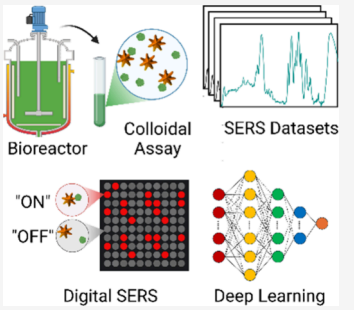

KEYWORDS: *deep learning, Raman spectroscopy, digital SERS, colloidal assay, cell culture media*

Maintaining consistent quality in biopharmaceutical manufacturing is essential for producing complex biologics, such as monoclonal antibodies, viral vectors, and cell therapies.[1] Even small variations in key process parameters or critical quality attributes can result in expensive batch failures, product recalls, and significant regulatory challenges.[2] To mitigate these risks, real-time process analytical technologies (PAT) are essential for monitoring key cell culture parameters, such as metabolite concentrations, and providing actionable feedback on critical process parameters (CPPs), including protein aggregation and glycosylation patterns.[3,4] However, current monitoring methods, such as high-performance liquid chromatography and mass spectrometry, are costly, require extensive offline analysis, and can introduce production delays of up to 48 h. These delays in real-time data capture and analysis create bottlenecks in bioprocess optimization and batch control, leading to inefficiencies and increased production costs.[5−7] Recent PAT advances in spectroscopic methods, capacitance sensors, and off-gas analyzers have provided a sophisticated degree of monitoring and control of both the bioreactor environment and cellular properties.[5] While offline sampling remains important due to its regulatory implications and its role in release testing, there is an urgent need for innovative PAT tools that can serve as an alternative and offer rapid, precise, and cost-effective analytical solutions to enhance biopharmaceutical manufacturing practices.

Raman spectroscopy is a nondestructive bioanalytical technique with high molecular specificity.[8,9] Its ability to monitor multiple molecules simultaneously, online and at-line, is particularly attractive as a PAT tool and in both upstream and downstream application.[10,11] Building on this capability, surface-enhanced Raman spectroscopy (SERS) leverages plasmonic nanostructures to boost weak Raman signals from lower-concentration analytes and provides the sensitivity required for detecting key metabolites, impurities, and other CPPs.[12,13] Nevertheless, conventional SERS suffers from considerable intensity fluctuations.[14−16] This can be attributed to various reasons, such as the inhomogeneous distribution of both hotspots and analytes on a plasmonic substrate,[17−21] as well as the highly dynamic analyte−metal interactions,[14−16] which compromises the achievable reproducibility. While single antibody-based spectro-immunoassays displayed strong capability to overcome the SERS intensity fluctuations by transducing frequency-shift signals based on nanomechanical perturbations of antibody-conjugated Raman molecules as a result of antibody−antigen interactions,[21−28] this approach can be hardly extended for label-free analysis of cell culture media.

Recently, a digital SERS protocol for chemical analysis[29,30] was proposed to overcome the SERS intensity fluctuation issues by converting SERS intensity signals into a digital binary signal in the form or "ON" or "OFF" based on a predefined intensity threshold. This effectively reduces false positives and

Received: February 17, 2025
Revised: March 23, 2025
Accepted: April 1, 2025
Published: April 3, 2025

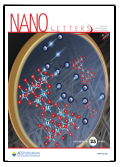

https://doi.org/10.1021/acs.nanolett.5c01071
Nano Lett. 2025, 25, 6284−6291

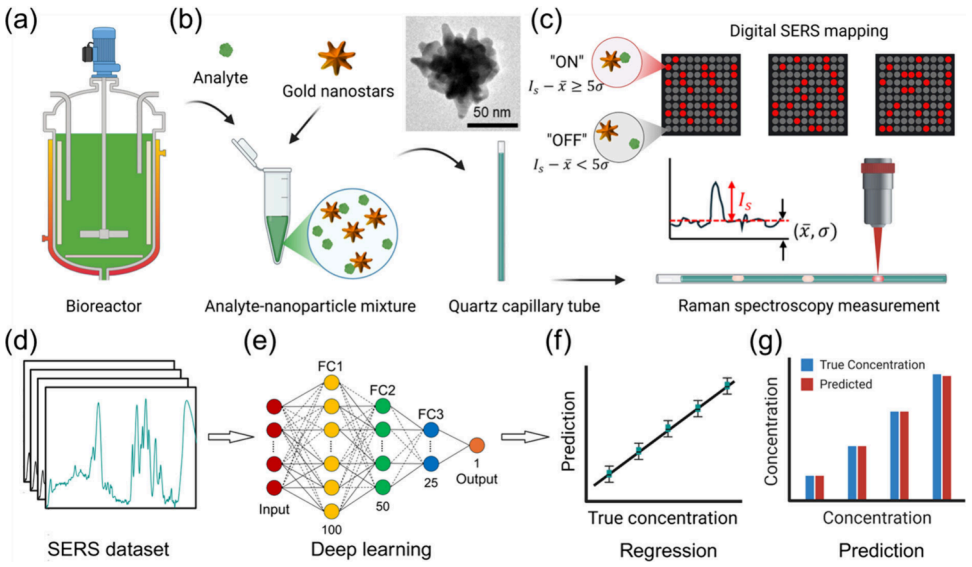

Figure 1. Scheme for deep learning-powered SERS for cell culture media monitoring. (a) Schematic of a bioreactor, (b) mixing of media analytes and colloidal gold nanostars (inset: a TEM image of a gold nanostar) and loading of the mixture into a quartz capillary tube, (c) protocol for Raman spectroscopy measurements and digital SERS analysis, (d) schematic of the SERS data set, (e) artificial neural network-based deep learning model, (f) regression analysis, and (g) concentration prediction. In (c), each map schematically indicates the area over which SERS spectra were collected from the quartz capillary tube.

allows digital visualization of single-molecule events, which significantly facilitates ultrasensitive detection of analytes, particularly at ultralow concentrations where the analyte–metal interactions primarily occur at the single-molecule level. Nevertheless, the performance of substrate-based digital SERS is predicated on rationally designed two-dimensional (2D) plasmonic substrates to maximize SERS enhancement[30] and, therefore, is still vulnerable to the inhomogeneous distribution of hotspots and analytes on the plasmonic substrate. Moreover, the short spatial decay length of the plasmonic fields perpendicular to the substrate limits the effective SERS enhancement to a very thin layer in close proximity to the surface of the substrate.[31] Additionally, the dewetting process of analytes on a substrate is time-consuming, often occurs in an uncontrolled manner, and could even prevent the analytes from being in close contact with the substrate owing to the difference in their respective surface energy. This further underscores the plethora of challenges confronting the substrate-based SERS arrays.

While 2D plasmonic substrates are constrained by those challenge, colloidal plasmonic nanoparticles could provide a highly reproducible liquid plasmonic platform for digital SERS analysis of various analytes owing to their colloidal homogeneity.[32−34] Given the stochastic nature of the interactions between colloidal nanoparticles and analytes, the digital SERS analysis can accurately capture positive nanoparticle–analyte interaction events and convert them into digital signals not directly affected by the absolute SERS intensity. Recent demonstrations of digital colloid-enhanced Raman spectroscopy validated the feasibility of colloidal digital SERS, where reproducible quantification of various analytes was demonstrated with single-molecule counting at very low concentrations, limited only by the Poisson noise of the measurement process.[35] Despite the promise, existing digital colloidal SERS is limited by the modest SERS enhancements from sphere-shaped gold nanoparticles and requires the analytes to possess a characteristic SERS peak, which significantly limits its applicability.

Herein, we propose to develop a deep learning-powered colloidal digital SERS assay by combining artificial intelligence with gold nanostar-based SERS spectroscopy. The enabling innovations of this integrated deep learning-SERS assay platform include the following: first, the homogeneous distribution of the colloidal plasmonic nanoparticles and analytes can deliver a high level of reproducibility, which remains elusive for substrate-based SERS assays. Second, the dynamic colloidal environment allows all the analytes to interact with the plasmonic nanoparticles based on concentration-correlated probability, allowing quantitative digital SERS analysis. In contrast, for substrate-based SERS assays, only these analytes located within the plasmonic field decay length can be effectively detected, while those beyond the decay length are largely missed in the acquired SERS spectra. Third, geometrically heterogeneous colloidal plasmonic nanoparticles, such as gold nanostars, possess significant SERS enhancements and wide spectral tunability, while the prevailing gold nanoparticles with a sphere shape can only provide a modest SERS enhancement with limited spectral tunability.[36,37] Fourth, digital SERS analysis circumvents the SERS intensity fluctuation issues and eliminates false signals. Leveraging the digital SERS counts to establish the correlation with the analyte concentration also enables single-molecule events to be accurately captured, which could be either missed because of limited sampling for substrate-based SERS assays or obscured by the background after averaging if the mean SERS intensity-based traditional approach was implemented. Fifth, the deep learning regression analysis leverages the artificial neural network (ANN) algorithm to predict the analyte concentration by extracting the hidden features based on studying the entire spectral features,[38−42] which, without relying on any characteristic peaks, significantly expands the applicability of the colloidal SERS assay. Ultimately, the integrated deep learning-powered colloidal digital SERS assay

https://doi.org/10.1021/acs.nanolett.5c01071
Nano Lett. 2025, 25, 6284−6291

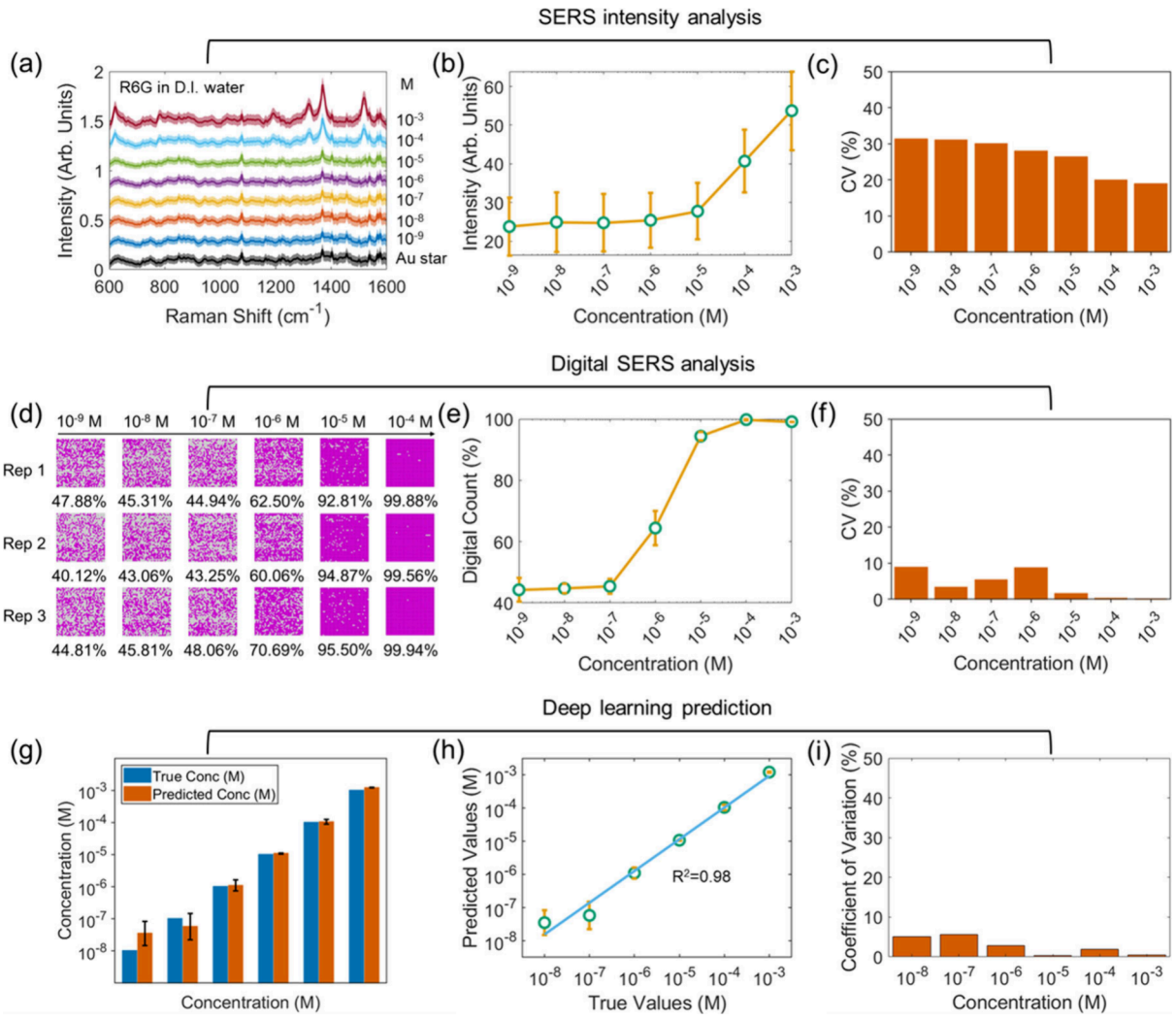

Figure 2. Colloidal SERS assay for detection of R6G in D.I. water. (a–c) SERS intensity analysis, where (a) represents the acquired raw SERS spectra with various R6G concentrations as specified, (b) the SERS intensity in relation to R6G concentration, and (c) the corresponding coefficient of variations (CV). (d–f) Digital SERS analysis, where (d) represents the distribution of digital SERS signals with various R6G concentrations across three repeats, (e) percentage of positive digital SERS counts in relation to the R6G concentration, and (f) the corresponding CV. (g–i) Deep learning analysis, where (g) represents the side-by-side comparison and (h) the correlation between the true and predicted concentrations, (i) the corresponding CV. In (d), each map (not in actual ratio) represents an area of 160 μm × 800 μm over which SERS spectra were collected from the quartz capillary tube. The digital SERS analysis was conducted using the characteristic SERS peak corresponding to the aromatic C–C stretching vibration at around 1520 cm^{-1}.

platform provides a highly promising and scalable strategy for rapid and accurate monitoring of various components in cell culture media.

Underpinning the colloidal digital SERS assay is the homogeneous colloidal mixture of cell culture media and gold nanostars (Figure 1a,b), where the gold nanostars were synthesized based on our previously reported approach.[21,43] The stochastic analyte–nanoparticle interactions produce temporal SERS intensity fluctuations. By converting each SERS spectrum based on a predefined intensity threshold using the characteristic SERS peak into a binary digital signal in the form of "ON" or "OFF", positive analyte–nanoparticle interactions can be accurately captured (Figure 1c). For instance, for a given analyte, if its SERS characteristic peak intensity I_s is equal to or higher than five times the standard deviation σ of the background as compared to the mean intensity of the background $\overline{x}$, this SERS spectrum is defined as a positive digital SERS count. Otherwise, a negative SERS count is returned. In this way, all the acquired SERS spectra can be converted into binary digital SERS signals. This effectively addresses the SERS intensity fluctuations by leveraging their stochastic nature while enabling digital visualization of single-molecule events.

While the obtained digital SERS count can be directly correlated with the analyte concentration to establish the calibration curve, deep learning offers a powerful alternative for detecting analytes that lack clear SERS signatures by analyzing the full spectral profile. Specifically, ANN is adopted to handle these high-dimensional SERS data sets (Figure 1d). The SERS data sets are first preprocessed by background removal using the fifth-order polynomial correction and normalized to properly scale the input features. Outliers are rejected using the robust principal component analysis (RPCA), which separates the SERS data sets into low-rank components that represent the underlying structure of the data and sparse components that capture outliers.[44,45] By applying a suitable

https://doi.org/10.1021/acs.nanolett.5c01071
Nano Lett. 2025, 25, 6284–6291

threshold to the sparse component, spectra with unexpected intensity fluctuations or artifacts are identified and removed. The cleaned SERS data sets are further split into training and testing subgroups using an 80−20 partition, where 80% of the cleaned data sets are allocated for training while the remaining 20% for testing. The 80−20 partition is a standard practice in deep learning that balances sufficient data for model training while reserving enough unseen data for reliable performance evaluation. Subsequently, the training data sets are fed into the input layer of the ANN architecture (Figure 1e). The input layer has the exact same number of features that correspond to that of input features in the cleaned SERS data set. The following three fully connected (FC) hidden layers are made to have a progressively decreasing number of artificial neurons, from 100, down to 50 and 25. Such a choice of the ANN architecture was made to balance model complexity and generalization, which promotes hierarchical feature extraction while minimizing the risk of overfitting. A rectified linear unit (ReLU) activation function is implemented to enable the extraction of nonlinear relationships and complex patterns in the SERS data set. During model training, the ANN is particularly tuned to recognize spectral features that vary systematically with analyte concentration, which enables accurate predictions even when distinct peaks are absent. As the ANN algorithm trains the model based on the labeled SERS data sets, it continuously adjusts the weights of each artificial neuron, which effectively optimizes its ability to predict the outcome for the unlabeled testing data sets. Eventually, the output layer has a single artificial neuron and returns the predicted value (Figure 1f,g). This data-driven approach allows the ANN to capture hidden spectral features and makes it highly effective for analyte detection even in complex or noisy SERS data sets.

To assess the performance of the deep learning-powered colloidal digital SERS assay platform, we started by implementing it to detect a standard Raman molecule, rhodamine 6G (R6G), in D.I. water. Following the protocol laid out in Figure 1, a series of R6G-gold nanostar colloidal mixtures with various R6G concentrations were first created and loaded into a quartz capillary tube for Raman spectroscopy measurements. A total of 1600 spectra were collected over a 160 μm × 800 μm area in about 16 min by a confocal Raman microscope at an excitation wavelength of 785 nm with an output laser power of approximately 4.3 μW. Each spectrum was collected with an acquisition time of 0.5 s. The mean SERS spectra were displayed in Figure 2a, where the shaded regions represent the standard deviation for the corresponding spectra collected at a given R6G concentration and the spectra were vertically offset for better visualization. We performed three types of data analysis, including the conventional SERS intensity analysis, digital SERS analysis, and deep learning analysis.

The conventional SERS intensity analysis was performed at the characteristic SERS peak at about 1520 cm^{-1}, which has an origin of the symmetric stretching mode of carbon−carbon bonds in the xanthene framework.[46] The mean peak intensity was found to decrease quickly with a decreasing R6G concentration (Figure 2b). Below 10^{-5} M, no further intensity change was observed. The coefficient of variation (CV) typically exceeded 20% (Figure 2c), which could be ascribed to the high dynamic nature of the R6G-gold nanostar interactions.

Furthermore, digital SERS analysis was performed using the same peak. For each concentration, we repeated the SERS measurement three times. For each measurement, the positive digital SERS count (%) was presented as the percentage. For each concentration, CV was calculated based on the three positive digital SERS counts (%). The converted digital SERS signals were spatially mapped across various concentrations and repeats, as presented in Figure 2d, where a gradual decrease of positive digital SERS counts was observed as the R6G concentration became lower. The mean digital SERS count was found to similarly decrease with a decreasing R6G concentration (Figure 2e), but with a lower detectable concentration down to 10^{-7} M as compared to the conventional SERS intensity analysis. Besides the observed lower detectable concentration, digital SERS analysis also returned a much lower CV, almost all of which are below 10% (Figure 2f). This suggests that a higher detection precision was achieved, which can be ascribed to the distinct advantage of digital SERS, which effectively suppressed background interference by assigning these signals as negative.

Additionally, deep learning analysis was conducted based on the ANN architecture to predict R6G concentrations. Through side-by-side comparison, the predicted concentrations were found to be consistently aligned closely with the true concentrations across all the studied concentration range down to 10^{-8} M (Figure 2g). Meanwhile, the predicted concentrations were found to correlate with the true concentration with a high coefficient of determination (R^2) value of 0.98 and small CVs that are all below 5%, as shown in Figure 2h,i. These observations underscore the accuracy of the ANN algorithm to capture complex nonlinear relationships by extracting the hidden features within the high-dimensional SERS data sets.

Taken together, the above analysis demonstrated the strong capability of both the digital SERS and deep learning, which displayed distinct advantages over conventional SERS intensity analysis, featuring a higher detection sensitivity and precision. Given the fact that not all analytes possess well-defined SERS peaks which precludes the possibility of digital SERS analysis, deep learning is thus expected to play a dominant role in detecting these analytes and can significantly expand the applicability of the colloidal SERS approach.

To demonstrate this approach's practical applicability, we extended it to detect key components of cell culture media, including glucose, tryptophan, and glutathione, which were dissolved in D.I. water, following the same protocol outlined in Figure 1. Digital SERS analysis successfully detected glucose and tryptophan with strong correlations between digital SERS counts and analyte concentrations (Figure 3a−d). Deep learning analysis of glutathione showed near-perfect alignment between predicted and true concentrations (Figure 3e,f), highlighting the method's versatility and sensitivity as an analytical platform. Importantly, for glutathione, the deep learning analysis overcame the limitations posed by the lack of well-defined SERS peaks. The observed high R^2 and low CV values validate the robustness of this approach for handling complex, high-dimensional data and highlight its ability to achieve sensitive and precise detection of diverse cell culture media components.

We further implement the deep learning-powered colloidal digital SERS for conducting rapid monitoring of cell culture media (AMBIC 1.1). The components and their concentrations in the AMBIC 1.1 media are detailed in Table S1. To

https://doi.org/10.1021/acs.nanolett.5c01071
Nano Lett. 2025, 25, 6284−6291

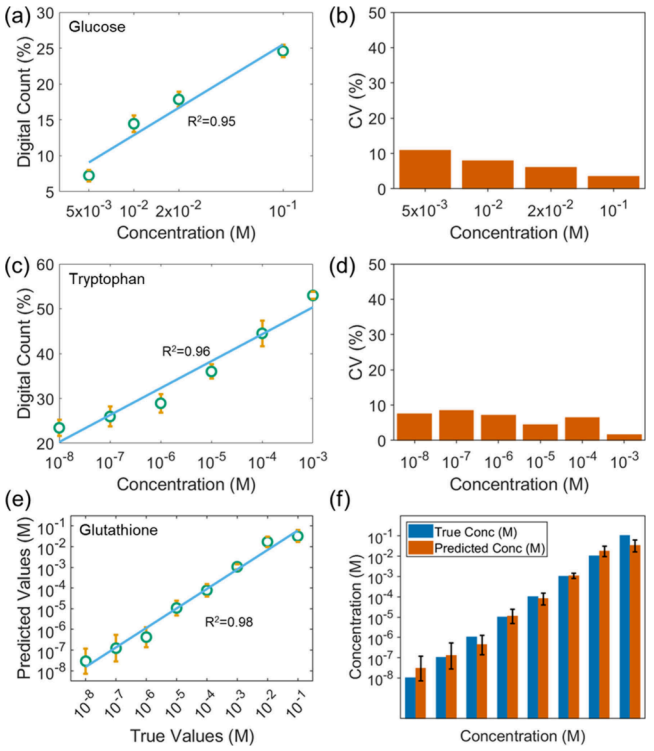

Figure 3. Digital SERS analysis of (a, b) glucose and (c, d) tryptophan, both in D.I. water. (e, f) Deep learning analysis of glutathione in D.I. water. For glucose and tryptophan, their respective characteristic SERS peaks at around 1125 cm^{-1} and 1365 cm^{-1} were utilized for digital SERS analysis. They have a respective origin of −C−O stretching and $-CH_2$ wagging and deformation.

perform a proof-of-concept demonstration, we selected three common analytes, including tryptophan, phenylalanine, and glucose. These analytes were individually spiked into fresh AMBIC 1.1 media, resulting in new media samples with known concentrations, which would allow us to systematically investigate the correlation between SERS signals and analyte levels. Analyte concentrations were evenly spaced on a log scale from the fresh media concentration up to the analytes' solubility limit. For example, when tryptophan was introduced into AMBIC 1.1 media in increasing amounts, three new samples were created, each with a higher concentration of tryptophan. The same approach was used for phenylalanine and glucose to ensure that we could measure a wide range of concentrations for each analyte.

The obtained SERS spectra are presented in Figure 4a,d,g. The characteristic SERS peak intensity displayed some variations to a certain extent in response to the analyte concentration increase. To quantify this relationship, we first employed the digital SERS approach. Figure 4b,e,h show that there was a robust linear correlation between the digital SERS counts and the concentration of each analyte across the measured range. Notably, the CV values for all three analytes are below 15%. Based on deep learning analysis, the predicted concentrations closely aligned with the actual concentrations across all samples, as shown in Figure 4c,f,i. Additionally, the feature importance calculations (Figure S4) indicate that the deep learning model was able to extract characteristic SERS spectral features even in the complex cell culture media. These results demonstrate the strong capability of the deep learning-powered colloidal digital SERS for precise, label-free monitoring of small-molecule cell culture media components. The precision and reproducibility of the method make it ideal

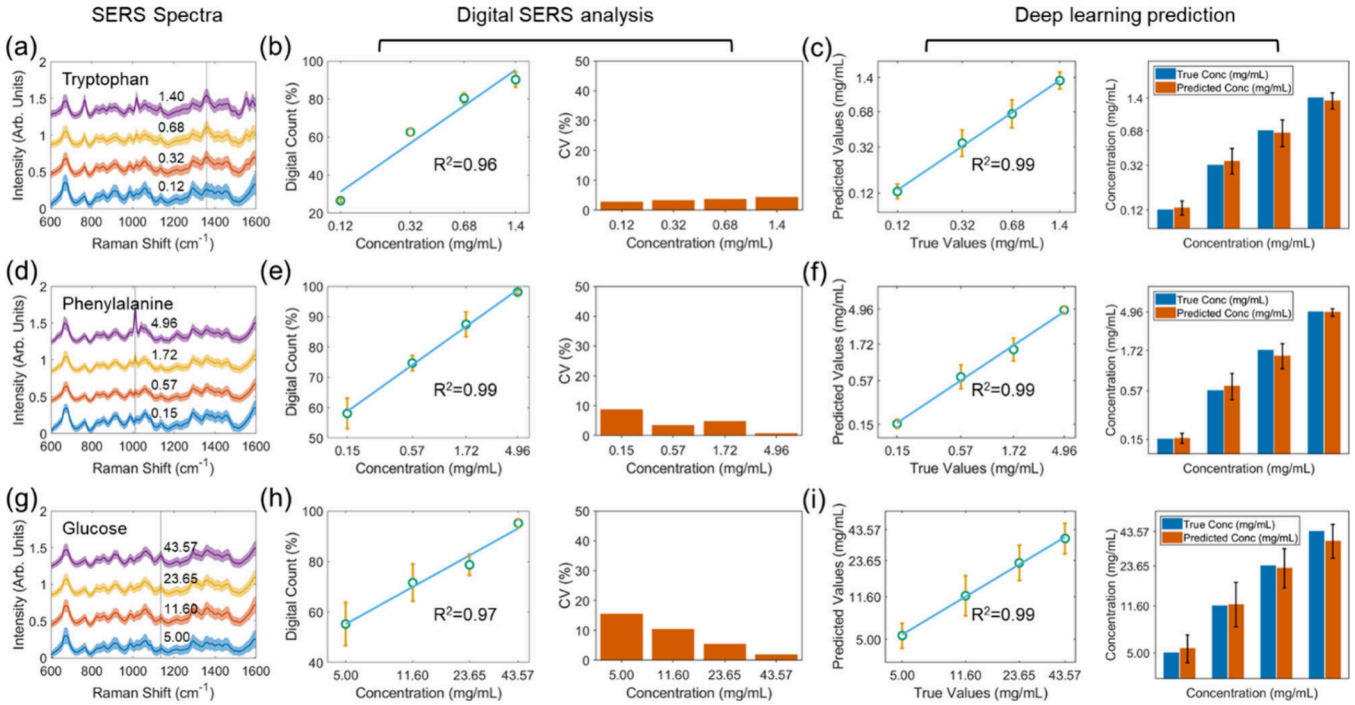

Figure 4. Cell culture media monitoring (AMBIC media 1.1). Detection of (a−c) tryptophan, (d−f) phenylalanine, and (g−i) glucose in cell culture media. For tryptophan, phenylalanine, and glucose, their respective characteristic SERS peaks utilized are at around 1365 cm^{-1}, 1005 cm^{-1}, and 1125 cm^{-1}. They have a respective origin of $-CH_2$ wagging and deformation, the phenyl ring symmetric breathing mode, and −C−O stretching. The calculated feature importance can be found in Figure S4, confirming their respective characteristic SERS peaks were extracted and utilized for deep learning analysis.

https://doi.org/10.1021/acs.nanolett.5c01071
Nano Lett. 2025, 25, 6284−6291

for real-time monitoring of cell culture component concentrations, which is critical for optimizing cell-based assays, biomanufacturing processes, and other biomedical applications.

As real-world biomanufacturing environments often involve complex mixtures where multiple analytes coexist at varying concentrations, deep learning-powered colloidal SERS offers distinct advantages due to its capacity to identify subtle spectral features that arise from overlapping signals. By training the ANN on mixed-analyte data sets, the model can effectively disentangle these complex spectral patterns and enable rapid, accurate quantification of individual analytes, further underscoring its vast potential in biomanufacturing.

In summary, we developed a deep learning-powered colloidal digital SERS platform for rapid and precise monitoring of cell culture media. By converting stochastic SERS intensity fluctuations into binary digital signals using the characteristic SERS peak, this method overcomes the limitations of conventional SERS, particularly the intensity fluctuations. By further leveraging deep learning for spectral analysis, the applicability of the approach is significantly expanded and can detect analytes even without well-defined SERS spectral peaks. This platform demonstrated superior sensitivity, reproducibility, and accuracy for detecting key analytes in both simple and complex cell culture media. Given the generalizability of this platform, we envision that this approach can be further scaled and adapted to monitor a broader range of analytes in various experimental conditions, opening up new possibilities for real-time, noninvasive monitoring in cell biology, as well as for large-scale, high-throughput screening assays and point-of-care diagnostic devices in clinical settings.

■ ASSOCIATED CONTENT

Supporting Information

The Supporting Information is available free of charge at https://pubs.acs.org/doi/10.1021/acs.nanolett.5c01071.

Details of materials and chemicals (Section S1), synthesis of gold nanostars (Section S2), microscopy and spectroscopy characterizations (Section S3), absorption spectrum for gold nanostars in water (Figure S1), raw SERS spectra for (a) glucose, (b) tryptophan, and (c) glutathione in D.I. water (Figure S2), the calculated coefficients of variations for glutathione in D.I. water (Figure S3), the calculated feature importance for tryptophan, phenylalanine, and glucose (Figure S4) (PDF)

■ AUTHOR INFORMATION

Corresponding Author

Ishan Barman − *Department of Mechanical Engineering, Johns Hopkins University, Baltimore, Maryland 21218, United States; Department of Oncology and The Russell H. Morgan Department of Radiology and Radiological Science, Johns Hopkins University School of Medicine, Baltimore, Maryland 21287, United States;* orcid.org/0000-0003-0800-0825; Email: ibarman@jhu.edu

Authors

Peng Zheng − *Department of Mechanical Engineering, Johns Hopkins University, Baltimore, Maryland 21218, United States;* orcid.org/0000-0001-5907-8505

Lintong Wu − *Department of Mechanical Engineering, Johns Hopkins University, Baltimore, Maryland 21218, United States*

Michael Ka Ho Lee − *Department of Mechanical Engineering, Johns Hopkins University, Baltimore, Maryland 21218, United States*

Andy Nelson − *Chemical and Biomolecular Engineering, Johns Hopkins University, Baltimore, Maryland 21218, United States*

Michael Betenbaugh − *Chemical and Biomolecular Engineering, Johns Hopkins University, Baltimore, Maryland 21218, United States;* orcid.org/0000-0002-1237-5550

Complete contact information is available at: https://pubs.acs.org/10.1021/acs.nanolett.5c01071

Notes

The authors declare the following competing financial interest(s): I.B. and P.Z. are inventors on the U.S. Application Number 63/743,671 filed by Johns Hopkins University.

■ ACKNOWLEDGMENTS

This work was supported by the National Institute of General Medical Sciences (1R35GM149272) and Advanced Mammalian Biomanufacturing Innovation Center (AMBIC).

■ REFERENCES

(1) Algorri, M.; Abernathy, M. J.; Cauchon, N. S.; Christian, T. R.; Lamm, C. F.; Moore, C. M. V. Re-Envisioning Pharmaceutical Manufacturing: Increasing Agility for Global Patient Access. *J. Pharm. Sci.* **2022**, *111* (3), 593−607.

(2) Gerzon, G.; Sheng, Y.; Kirkitadze, M. Process Analytical Technologies − Advances in bioprocess integration and future perspectives. *J. Pharm. Biomed. Anal.* **2022**, *207*, No. 114379.

(3) Campbell, A.; Brieva, T.; Raviv, L.; Rowley, J.; Niss, K.; Brandwein, H.; Oh, S.; Karnieli, O. Concise Review: Process Development Considerations for Cell Therapy. *Stem Cells Translational Medicine* **2015**, *4* (10), 1155−1163.

(4) Iancu, E. M.; Kandalaft, L. E. Challenges and advantages of cell therapy manufacturing under Good Manufacturing Practices within the hospital setting. *Curr. Opin. Biotechnol.* **2020**, *65*, 233−241.

(5) Gillespie, C.; Wasalathanthri, D. P.; Ritz, D. B.; Zhou, G.; Davis, K. A.; Wucherpfennig, T.; Hazelwood, N. Systematic assessment of process analytical technologies for biologics. *Biotechnol. Bioeng.* **2022**, *119* (2), 423−434.

(6) Bolje, A.; Gobec, S. Analytical Techniques for Structural Characterization of Proteins in Solid Pharmaceutical Forms: An Overview. *Pharmaceutics* **2021**, *13*, 534.

(7) Simon, L. L.; Pataki, H.; Marosi, G.; Meemken, F.; Hungerbühler, K.; Baiker, A.; Tummala, S.; Glennon, B.; Kuentz, M.; Steele, G.; Kramer, H. J. M.; Rydzak, J. W.; Chen, Z.; Morris, J.; Kjell, F.; Singh, R.; Gani, R.; Gernaey, K. V.; Louhi-Kultanen, M.; O'Reilly, J.; Sandler, N.; Antikainen, O.; Yliruusi, J.; Frohberg, P.; Ulrich, J.; Braatz, R. D.; Leyssens, T.; von Stosch, M.; Oliveira, R.; Tan, R. B. H.; Wu, H.; Khan, M.; O'Grady, D.; Pandey, A.; Westra, R.; Delle-Case, E.; Pape, D.; Angelosante, D.; Maret, Y.; Steiger, O.; Lenner, M.; Abbou-Oucherif, K.; Nagy, Z. K.; Litster, J. D.; Kamaraju, V. K.; Chiu, M.-S. Assessment of Recent Process Analytical Technology (PAT) Trends: A Multiauthor Review. *Org. Process Res. Dev.* **2015**, *19* (1), 3−62.

(8) Dodo, K.; Fujita, K.; Sodeoka, M. Raman Spectroscopy for Chemical Biology Research. *J. Am. Chem. Soc.* **2022**, *144* (43), 19651−19667.

(9) Zong, C.; Xu, M.; Xu, L.-J.; Wei, T.; Ma, X.; Zheng, X.-S.; Hu, R.; Ren, B. Surface-Enhanced Raman Spectroscopy for Bioanalysis: Reliability and Challenges. *Chem. Rev.* **2018**, *118* (10), 4946−4980.

(10) Esmonde-White, K. A.; Cuellar, M.; Uerpmann, C.; Lenain, B.; Lewis, I. R. Raman spectroscopy as a process analytical technology for pharmaceutical manufacturing and bioprocessing. *Anal. Bioanal. Chem.* **2017**, *409* (3), 637−649.
(11) Zhan, C.; Chen, X.-J.; Yi, J.; Li, J.-F.; Wu, D.-Y.; Tian, Z.-Q. From plasmon-enhanced molecular spectroscopy to plasmon-mediated chemical reactions. *Nature Reviews Chemistry* **2018**, *2* (9), 216−230.
(12) Langer, J.; Jimenez de Aberasturi, D.; Aizpurua, J.; Alvarez-Puebla, R. A.; Auguié, B.; Baumberg, J. J.; Bazan, G. C.; Bell, S. E. J.; Boisen, A.; Brolo, A. G.; Choo, J.; Cialla-May, D.; Deckert, V.; Fabris, L.; Faulds, K.; García de Abajo, F. J.; Goodacre, R.; Graham, D.; Haes, A. J.; Haynes, C. L.; Huck, C.; Itoh, T.; Käll, M.; Kneipp, J.; Kotov, N. A.; Kuang, H.; Le Ru, E. C.; Lee, H. K.; Li, J.-F.; Ling, X. Y.; Maier, S. A.; Mayerhöfer, T.; Moskovits, M.; Murakoshi, K.; Nam, J.-M.; Nie, S.; Ozaki, Y.; Pastoriza-Santos, I.; Perez-Juste, J.; Popp, J.; Pucci, A.; Reich, S.; Ren, B.; Schatz, G. C.; Shegai, T.; Schlücker, S.; Tay, L.-L.; Thomas, K. G.; Tian, Z.-Q.; Van Duyne, R. P.; Vo-Dinh, T.; Wang, Y.; Willets, K. A.; Xu, C.; Xu, H.; Xu, Y.; Yamamoto, Y. S.; Zhao, B.; Liz-Marzán, L. M. Present and Future of Surface-Enhanced Raman Scattering. *ACS Nano* **2020**, *14* (1), 28−117.
(13) Pérez-Jiménez, A. I.; Lyu, D.; Lu, Z.; Liu, G.; Ren, B. Surface-enhanced Raman spectroscopy: benefits, trade-offs and future developments. *Chemical Science* **2020**, *11* (18), 4563−4577.
(14) Lindquist, N. C.; de Albuquerque, C. D. L.; Sobral-Filho, R. G.; Paci, I.; Brolo, A. G. High-speed imaging of surface-enhanced Raman scattering fluctuations from individual nanoparticles. *Nat. Nanotechnol.* **2019**, *14* (10), 981−987.
(15) Almehmadi, L. M.; Curley, S. M.; Tokranova, N. A.; Tenenbaum, S. A.; Lednev, I. K. Surface Enhanced Raman Spectroscopy for Single Molecule Protein Detection. *Sci. Rep.* **2019**, *9* (1), No. 12356.
(16) Natan, M. J. Concluding Remarks Surface enhanced Raman scattering. *Faraday Discuss.* **2006**, *132* (0), 321−328.
(17) Zhao, Y.; Mukherjee, K.; Benkstein, K. D.; Sun, L.; Steffens, K. L.; Montgomery, C. B.; Guo, S.; Semancik, S.; Zaghloul, M. E. Miniaturized nanohole array based plasmonic sensor for the detection of acetone and ethanol with insights into the kinetics of adsorptive plasmonic sensing. *Nanoscale* **2019**, *11* (24), 11922−11932.
(18) Zhao, Y.; Dong, B.; Benkstein, K. D.; Chen, L.; Steffens, K. L.; Semancik, S. Deep Learning Image Analysis of Nanoplasmonic Sensors: Toward Medical Breath Monitoring. *ACS Appl. Mater. Interfaces* **2022**, *14* (49), 54411−54422.
(19) Zheng, P.; Cushing, S. K.; Suri, S.; Wu, N. Tailoring plasmonic properties of gold nanohole arrays for surface-enhanced Raman scattering. *Phys. Chem. Chem. Phys.* **2015**, *17* (33), 21211−21219.
(20) Zheng, P.; Kasani, S.; Shi, X.; Boryczka, A. E.; Yang, F.; Tang, H.; Li, M.; Zheng, W.; Elswick, D. E.; Wu, N. Detection of nitrite with a surface-enhanced Raman scattering sensor based on silver nanopyramid array. *Anal. Chim. Acta* **2018**, *1040*, 158−165.
(21) Zheng, P.; Kasani, S.; Tan, W.; Boryczka, J.; Gao, X.; Yang, F.; Wu, N. Plasmon-enhanced near-infrared fluorescence detection of traumatic brain injury biomarker glial fibrillary acidic protein in blood plasma. *Anal. Chim. Acta* **2022**, *1203*, No. 339721.
(22) Kho, K. W.; Dinish, U. S.; Kumar, A.; Olivo, M. Frequency Shifts in SERS for Biosensing. *ACS Nano* **2012**, *6* (6), 4892−4902.
(23) Penas, C.; Pazos, E.; Mascareñas, J. L.; Vázquez, M. E. A Folding-Based Approach for the Luminescent Detection of a Short RNA Hairpin. *J. Am. Chem. Soc.* **2013**, *135* (10), 3812−3814.
(24) Ma, H.; Liu, S.; Zheng, N.; Liu, Y.; Han, X. X.; He, C.; Lu, H.; Zhao, B. Frequency Shifts in Surface-Enhanced Raman Spectroscopy-Based Immunoassays: Mechanistic Insights and Application in Protein Carbonylation Detection. *Anal. Chem.* **2019**, *91* (15), 9376−9381.
(25) Zhu, W.; Wang, Y.; Xie, D.; Cheng, L.; Wang, P.; Zeng, Q.; Li, M.; Zhao, Y. In Situ Monitoring the Aggregation Dynamics of Amyloid-β Protein Aβ42 in Physiological Media via a Raman-Based Frequency Shift Method. *ACS Applied Bio Materials* **2018**, *1* (3), 814−824.
(26) Zheng, P.; Wu, L.; Raj, P.; Kim, J. H.; Paidi, S. K.; Semancik, S.; Barman, I. Multiplexed SERS Detection of Serum Cardiac Markers Using Plasmonic Metasurfaces. *Advanced Science* **2024**, *11* (45), No. 2405910.
(27) Zheng, P.; Raj, P.; Wu, L.; Mizutani, T.; Szabo, M.; Hanson, W. A.; Barman, I. Quantitative Detection of Thyroid-Stimulating Hormone in Patient Samples with a Nanomechanical Single-Antibody Spectro-Immunoassay. *Small* **2024**, *20* (6), No. 2305110.
(28) Zheng, P.; Raj, P.; Wu, L.; Szabo, M.; Hanson, W. A.; Mizutani, T.; Barman, I. Leveraging Nanomechanical Perturbations in Raman Spectro-Immunoassays to Design a Versatile Serum Biomarker Detection Platform. *Small* **2022**, *18* (42), No. 2204541.
(29) de Albuquerque, C. D. L.; Sobral-Filho, R. G.; Poppi, R. J.; Brolo, A. G. Digital Protocol for Chemical Analysis at Ultralow Concentrations by Surface-Enhanced Raman Scattering. *Anal. Chem.* **2018**, *90* (2), 1248−1254.
(30) Zheng, P.; Wu, L.; Barman, I. Plasmonic Gold Prism Array for Digital Surface-Enhanced Raman Spectroscopy Sensing. *J. Phys. Chem. C* **2024**, *128* (34), 14375−14380.
(31) Bhalla, N.; Shen, A. Q. Localized Surface Plasmon Resonance Sensing and its Interplay with Fluidics. *Langmuir* **2024**, *40* (19), 9842−9854.
(32) Hsu, S.-W.; Rodarte, A. L.; Som, M.; Arya, G.; Tao, A. R. Colloidal Plasmonic Nanocomposites: From Fabrication to Optical Function. *Chem. Rev.* **2018**, *118* (6), 3100−3120.
(33) Ha, M.; Kim, J.-H.; You, M.; Li, Q.; Fan, C.; Nam, J.-M. Multicomponent Plasmonic Nanoparticles: From Heterostructured Nanoparticles to Colloidal Composite Nanostructures. *Chem. Rev.* **2019**, *119* (24), 12208−12278.
(34) Comin, A.; Manna, L. New materials for tunable plasmonic colloidal nanocrystals. *Chem. Soc. Rev.* **2014**, *43* (11), 3957−3975.
(35) Bi, X.; He, Z.; Luo, Z.; Huang, W.; Diao, X.; Ye, J. Digital colloid-enhanced Raman spectroscopy for the pharmacokinetic detection of bioorthogonal drugs. *Chemical Science* **2024**, *15* (34), 13998−14008.
(36) Li, M.; Cushing, S. K.; Zhang, J.; Lankford, J.; Aguilar, Z. P.; Ma, D.; Wu, N. Shape-dependent surface-enhanced Raman scattering in gold−Raman-probe−silica sandwiched nanoparticles for biocompatible applications. *Nanotechnology* **2012**, *23* (11), No. 115501.
(37) Pu, Y.; Zhao, Y.; Zheng, P.; Li, M. Elucidating the Growth Mechanism of Plasmonic Gold Nanostars with Tunable Optical and Photothermal Properties. *Inorg. Chem.* **2018**, *57* (14), 8599−8607.
(38) Lussier, F.; Thibault, V.; Charron, B.; Wallace, G. Q.; Masson, J.-F. Deep learning and artificial intelligence methods for Raman and surface-enhanced Raman scattering. *TrAC Trends in Analytical Chemistry* **2020**, *124*, No. 115796.
(39) Hinton, G. E.; Salakhutdinov, R. R. Reducing the Dimensionality of Data with Neural Networks. *Science* **2006**, *313* (5786), 504−507.
(40) Hopfield, J. J.; Tank, D. W. Computing with Neural Circuits: A Model. *Science* **1986**, *233* (4764), 625−633.
(41) Guselnikova, O.; Trelin, A.; Skvortsova, A.; Ulbrich, P.; Postnikov, P.; Pershina, A.; Sykora, D.; Svorcik, V.; Lyutakov, O. Label-free surface-enhanced Raman spectroscopy with artificial neural network technique for recognition photoinduced DNA damage. *Biosens. Bioelectron.* **2019**, *145*, No. 111718.
(42) Trelin, A.; Skvortsova, A.; Olshtrem, A.; Chertopalov, S.; Mares, D.; Lapcak, L.; Vondracek, M.; Sajdl, P.; Jerabek, V.; Maixner, J.; Lancok, J.; Sofer, Z.; Regner, J.; Kolska, Z.; Svorcik, V.; Lyutakov, O. Surface-Enhanced Raman Spectroscopy and Artificial Neural Networks for Detection of MXene Flakes' Surface Terminations. *J. Phys. Chem. C* **2024**, *128* (16), 6780−6787.
(43) Zheng, P.; Kang, J.; Paria, D.; Kang, J. U.; Barman, I. Molecular Radiative Energy Shifts under Strong Oscillating Fields. *Small* **2021**, *17* (3), No. 2007244.
(44) Cai, H.; Liu, J.; Yin, W. Learned robust PCA: A scalable deep unfolding approach for high-dimensional outlier detection. *Advances in Neural Information Processing Systems* **2021**, *34*, 16977−16989.

https://doi.org/10.1021/acs.nanolett.5c01071
Nano Lett. 2025, 25, 6284−6291

(45) Jin, Z.-F.; Wang, Q.; Wan, Z. Recovering low-rank matrices from corrupted observations via the linear conjugate gradient algorithm. *Journal of computational and applied mathematics* **2014**, *256*, 114−120.
(46) Watanabe, H.; Hayazawa, N.; Inouye, Y.; Kawata, S. DFT Vibrational Calculations of Rhodamine 6G Adsorbed on Silver: Analysis of Tip-Enhanced Raman Spectroscopy. *J. Phys. Chem. B* **2005**, *109* (11), 5012−5020.

https://doi.org/10.1021/acs.nanolett.5c01071
Nano Lett. 2025, 25, 6284−6291